ASCE

Methodology for Regularization of Force-Based Elements to Model Reinforced Concrete Columns with Short Lap Splices

Yijian Zhang, P.E., M.ASCE[1]; and Iris Tien, Ph.D.[2]

Abstract: In reinforced concrete structures built before the 1970s, it was common for columns to be constructed with short lap splices and widely spaced transverse bars at the column base, leading to increased likelihoods of pull-out failures and structural collapse during seismic events. In the modeling and analysis of reinforced concrete columns with short lap splices, several challenges arise, particularly with softening behavior that leads to strain localization and scaling and convergence issues in analyses. This research presents a methodology to regularize force-based beam-column elements with softening lap-splice material response. In the methodology, a constant energy release criterion is imposed with the constant postpeak energy of the lap-splice region determined from relevant experimental data. With the proposed regularization, the numerical model shows objective results that are independent of the length of the element and number of integration points used. Whereas the accuracy in estimating, for example, the displacement at 20% strength drop using existing nonregularized models changes with the number of integration points, the accuracy using the proposed model remains constant across numbers of integration points used with a mean accuracy of 94% compared with experimental tests. Results from static pushover and cyclic analyses show an order of magnitude decrease in standard deviation of the response using the regularized model. Increased accuracy and increased convergence for the method across the number of integration points used is shown in static and dynamic analyses. The proposed regularization approach is able to alleviate strain localization issues and facilitates the scaling of analyses from small-scale to full-scale structures. **DOI: 10.1061/(ASCE)EM.1943-7889.0001778.**

Introduction

In older structures, including both buildings (Melek and Wallace 2004; Cho and Pincheira 2006) and highway bridges (Chail et al. 1991; Sun et al. 1993) built pre-1970s, it was common for reinforced concrete columns to consist of widely spaced transverse reinforcement and short lap splices at the base of the column with lap length of 20–24 times the longitudinal bar diameter. Structures with short lap splices at the base have limited ductility and lateral strength. These structures more likely to exhibit poor performance under lateral loadings, and have an increased probability of suffering damage during seismic events. Damage includes potential pull-out failures and even structural collapse.

To assess the performance of these structures, nonlinear analysis is becoming common practice to predict and evaluate responses. Having accurate and consistent numerical models is essential to conduct these analyses and capture the failure mechanisms of columns with short lap splices. However, existing approaches are not objective due to the softening characteristic of the force-transferring mechanism between the concrete and lap-splice bars. In columns with short lap splices, behavior in the lap-splice region governs column response, which in turn often governs overall structural response. Therefore, objective models for these analyses, including of the lap-spliced material, which are independent of the number of integration points and do not suffer from length scale issues are needed.

In the numerical modeling of reinforced concrete columns presented in this paper, two elements are used with the bottom element covering the length of the lap splice. Using two elements rather than a single element enables the distribution of plasticity along the lap-splice region to be captured. In the bottom element, previous studies have suggested use of two integration points (Tariverdilo et al. 2009), leading to numerical results that correspond closely with experimental tests. However, as the length of a specimen increases, including from lab-scale test specimens to full-scale columns, increasing the number of integration points may be desired to capture the behavior along the lap splice. Changing the number of integration points leads to strain localization issues, resulting in inaccurate element response outcomes from the model. For example, the resulting element flexibility matrix and corresponding stiffness matrix, as well as element rotational and axial deformations, change based on the number of integration points used, leading to inaccuracies in the analysis results.

In addition, results even with two integration points may be inaccurate for some specimens, as shown subsequently in this study. Therefore, there is the need for an approach that is able to obtain accurate and consistent analysis results that are independent of the length of the element and independent of the number of integration points used. The proposed regularization approach results in objective numerical models. This study describes and evaluates the regularization approach that uses a constant postpeak energy criterion for reinforced concrete columns with short lap splices.

The rest of the paper is organized as follows. The next section provides background and related studies motivating this work.

[1]Graduate Research Assistant, School of Civil and Environmental Engineering, Georgia Institute of Technology, 790 Atlantic Dr, Atlanta, GA 30332 (corresponding author). Email: zyj.albert@gatech.edu

[2]Asistant Professor, School of Civil and Environmental Engineering, Georgia Institute of Technology, 790 Atlantic Dr., Atlanta, GA 30332. ORCID: https://orcid.org/0000-0002-1410-632X. Email: itien@ce.gatech.edu

Note. This manuscript was submitted on May 24, 2019; approved on December 31, 2019; published online on April 30, 2020. Discussion period open until September 30, 2020; separate discussions must be submitted for individual papers. This paper is part of the ***Journal of Engineering Mechanics***, © ASCE, ISSN 0733-9399.

The following section presents the formulation of the force-based numerical element. The proposed regularization procedure for the lap splice due to local softening behavior in tension is then presented. The modeling details for the columns analyzed using force-based beam-column elements are provided. The next section shows the results from using the proposed regularized compared to non-regularized model. Results include verification of the numerical model against experimental tests and convergence results for static and dynamic analyses considering varying numbers of integration points in the lap-splice region.

Background and Related Work

There have been several previous analytical studies of the nonlinear response of columns with short lap splices (Reyes and Pincheira 1999; Cho and Pincheira 2006; Tariverdilo et al. 2009). Cho and Pincheira (2006) proposed an analytical modeling approach using nonlinear rotational springs at the element end to model the degradation of stiffness and strength with increasing deformation amplitude. Even though the model is numerically efficient by taking advantage of a concentrated plasticity modeling approach, it requires the user to obtain the parameters to define the nonlinear rotational springs from other sources, e.g., through experimental tests. Tariverdilo et al. (2009) presented a model that is able to capture the degrading response due to bar slip in the lap splice based on the configuration and yield stress of the longitudinal reinforcement and the spacing and amount of transverse reinforcement. The model showed good correlation with results from experimental tests. However, because the degrading mechanism in Tariverdilo et al. (2009)'s model due to bar slip is manifested through the softening stress-strain relation at the material level in the force-based beam-column element, loss of objectivity due to strain localization has become critical in the numerical modeling and analysis.

Previous studies (e.g., Tariverdilo et al. 2009) suggested the use of two Gauss-Lobatto integration points within the lap-spliced element to model the response of short lap splices regardless of the length of the splice. The selection of two integration points is ambiguous from a numerical standpoint because the integration length of the lap-splice region could change as the length of the element changes, for example, between a test specimen and full-scale structural column. The assumption of using two integration points can thus impact the accuracy of the numerical model in predicting the response of a real structural column subject to lap-splice failure. The loss of objectivity has also been shown in other studies, where the number of integration points used in the force-based element dictates the response of the model at the location of softening constitutive behavior (Coleman and Spacone 2001; Addessi and Ciampi 2007; Scott and Hamutçuoğlu 2008). The variation in results with different numbers of integration points further leads to accuracy and convergence issues in the analysis.

This paper presents a methodology to address the issue of strain localization for columns with short lap splices through regularization based on a constant postpeak energy criterion. Previous studies have used the concept of constant fracture energy to address mesh-sensitivity issues in displacement-based continuum finite-element analyses due to the softening response for concrete in tension (Bažant and Oh 1983; Bazant and Planas 1997). The concept of a constant energy criterion has been extended to the softening response in compression (Jansen and Shah 1997; Lee and William 1997). Several studies have investigated the issue of strain localization specifically for force-based frame elements (Coleman and Spacone 2001; Addessi and Ciampi 2007; Scott and Hamutçuoğlu 2008). In particular, Coleman and Spacone (2001) showed that for modeling a reinforced column with a single force-based element, the force-displacement response loses its objectivity and varies based on the number of integration points used. In the presence of strain softening behavior of crushing concrete, strain rapidly increases in the extreme fiber as the response proceeds in the post-peak region. Despite these studies investigating strain localization due to the nonlinear concrete response in compression, there is no study delving into the localized phenomenon that occurs in reinforced concrete columns with short lap splices due to the bond slip mechanism. This study alleviates strain localization effects through regularizing the lap-splice material response. The numerical model utilizing the proposed approach shows objective and accurate results compared with experimental values and consistent results that converge across varying numbers of integration points.

Proposed Methodology

Formulation of Force-Based Element

Force-based elements described by Spacone et al. (1996a, b) have been widely used by the structural engineering community for nonlinear finite element analysis. Fig. 1 shows the force and element deformation in the basic frame [Fig. 1(a)] and global frame [Fig. 1(b)] (Filippou and Fenves 2004), where $\mathbf{q}$, $\mathbf{v}$ and $\bar{\mathbf{q}}$, $\bar{\mathbf{v}}$ represent force and element deformation in the natural frame and global frame, respectively.

Compared with displacement-based elements with interpolation of the displacement field, force-based elements utilize the interpolation functions $\mathbf{b}(x)$ of basic forces $\mathbf{q}$ within the basic system. The product of interpolation functions and basic forces results in sectional forces $\mathbf{s}(x)$ consisting of axial force and moment located at distance $\mathbf{x}$ from one end of an element node. Under Euler-Bernoulli beam theory, sectional deformation $\mathbf{e}$ consists of only axial strain and curvature for the sectional response. In the absence of element loading, Eq. (1*a*) shows the relation between basic element and sectional forces

$$\mathbf{s}(x) = \mathbf{b}(x)\mathbf{q} \tag{1a}$$

Eq. (1*a*) can be also expressed explicitly as in Eq. (1*b*)

$$\begin{bmatrix} N(x) \\ M(x) \end{bmatrix} = \begin{bmatrix} 1 & 0 & 0 \\ 0 & \frac{x}{L} - 1 & \frac{x}{L} \end{bmatrix} \begin{bmatrix} q_1 \\ q_2 \\ q_3 \end{bmatrix} \tag{1b}$$

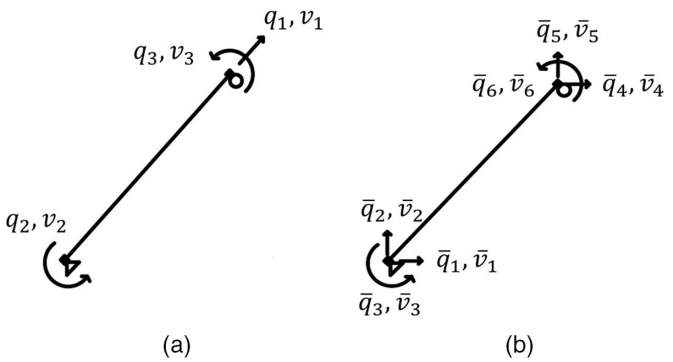

Fig. 1. Degrees of freedom: (a) basic frame; and (b) global frame.

where q_1, q_2, and q_3 = axial force and end moments of the line element; L = length of the element; and $N(x)$ and $M(x)$ = sectional forces at distance x from one end of the element node. According to the principle of virtual force, virtual sectional forces $\delta\mathbf{s}$ and sectional deformation $\mathbf{e}$ can be related to virtual element basic forces $\delta\mathbf{q}$ and element deformation $\mathbf{v}$ as shown in Eq. (2)

$$\delta\mathbf{q}^T\mathbf{v} = \int_0^L \delta\mathbf{s}(x)^T\mathbf{e}(x)dx \tag{2}$$

By considering Eq. (1*a*) in the virtual force system and Eq. (2), Eq. (3) establishes the relation between element deformation $\mathbf{v}$ and sectional deformation $\mathbf{e}$

$$\mathbf{v} = \int_0^L \mathbf{b}(x)^T\mathbf{e}(x)dx \tag{3}$$

Element flexibility matrix $\mathbf{f_e}$ is obtained by taking the derivative of Eq. (3) with respect to basic forces $\mathbf{q}$ as shown in Eqs. (4*a*) and (4*b*)

$$\mathbf{f_e} = \frac{\partial}{\partial\mathbf{q}}\int_0^L \mathbf{b}(x)^T\mathbf{e}(x)dx \tag{4a}$$

$$\mathbf{f_e} = \int_0^L \mathbf{b}(x)^T\frac{\partial\mathbf{e}(x)}{\partial\mathbf{s}}\frac{\partial\mathbf{s}}{\partial\mathbf{q}}dx \tag{4b}$$

Element flexibility matrix $\mathbf{f_e}$ is derived in terms of sectional flexibility matrix $\mathbf{f_s}$ and interpolation function $\mathbf{b}(x)$ as shown in Eq. (5)

$$\mathbf{f_e} = \int_0^L \mathbf{b}(x)^T\mathbf{f_s}\mathbf{b}(x)dx \tag{5}$$

Finally, element stiffness matrix $\mathbf{k_e}$ is obtained by inversion of the element flexibility matrix. The force formulation enables equilibrium between sectional forces and element forces, and compatibility between sectional deformation and element deformation is satisfied in an integral sense.

Eqs. (3) and (5) are evaluated through numerical integration according to Eqs. (6) and (7), respectively. The authors adopt the Gauss-Lobatto integration scheme, which evaluates end points of the structural element where the maximum moment occurs in the absence of element loading

$$\mathbf{v} \cong \sum_{\mathrm{IP}=1}^{N} \mathbf{b}(x_{\mathrm{IP}})^T\mathbf{e}(x_{\mathrm{IP}})Lw_{\mathrm{IP}} \tag{6}$$

$$\mathbf{f_e} \cong \sum_{\mathrm{IP}=1}^{N} \mathbf{b}(x_{\mathrm{IP}})^T\mathbf{f_s}\mathbf{b}(x_{\mathrm{IP}})Lw_{\mathrm{IP}} \tag{7}$$

where w_{IP} and x_{IP} = weight and position, respectively, for a particular integration point (IP). The domain for the integration weight w_{IP} is between 0 and 1; the domain for the position x_{IP} is between 0 and element length L. The product of L and w_{IP} is defined as L_{IP}, the length associated with an integration point. N is the total number of integration points along the element.

The element response is dependent on L_{IP}, and the loss of objectivity that this paper addresses arises when the number of integration points changes along each element in the presence of softening material response and when the length L_{IP} changes. This paper proposes to regularize the lap-splice material response through a constant energy criterion. Specifically, the material model for the lap-spliced section is modified based on a constant postpeak energy value obtained from experimental tests and tied to the element response through Eqs. (6) and (7) to regularize the element response.

Regularization of Material Constitutive Model

The following two sections detail the regularization of the material response for concrete in compression and the softening response of a lap splice in tension. In a force-based beam-column model with fiber sections, regularization of the material uniaxial response deliberately increases the energy per length in the one-dimensional (1D) constitutive relation as the number of integration points increases along the element in order to achieve constant energy release. During the regularization process in this study, the regularized strain is modified to a larger value as the number of integration points increases in the lapped region. This artificial increase of strain produces additional energy per length enclosed by the modified stress-strain curve at the material level. However, the total energy release remains constant due to the reduction of the integration length. The regularization is implemented through adjusting the degrading slope after the peak stress. The increase of slope (i.e., having a less negative degrading slope) creates additional sectional stiffness $\widetilde{\mathbf{k}_s}$ as shown in Eq. (8). As a result, the total sectional stiffness $\widetilde{\mathbf{k}_s}$ increases, leading to a reduction of the sectional deformation $\boldsymbol{e}$ and sectional flexibility $\mathbf{f_s}$. Finally, the stabilization of the element response is achieved through stabilizing the element deformation $\mathbf{v}$ by adjusting the value of the sectional deformation $\mathbf{e}$ based on Eq. (6)

$$\widehat{\mathbf{k}_s} = \int \mathbf{a}_s^T\left(\widehat{\frac{\partial\sigma}{\partial\varepsilon}}\right)\mathbf{a}_s dA = \int \mathbf{a}_s^T\left(\frac{\partial\sigma}{\partial\varepsilon}\right)\mathbf{a}_s dA + \int \mathbf{a}_s^T\left(\widetilde{\frac{\partial\sigma}{\partial\varepsilon}}\right)\mathbf{a}_s dA \tag{8a}$$

$$\widehat{\mathbf{k}_s} = \mathbf{k}_s + \widetilde{\mathbf{k}_s} \tag{8b}$$

where $\partial\sigma/\partial\varepsilon$ = original tangent material stiffness of the softening portion; $\widehat{\partial\sigma/\partial\varepsilon}$ = regularized tangent material stiffness of the softening portion; $\widetilde{\partial\sigma/\partial\varepsilon}$ = additional contribution of the tangent material stiffness of the softening portion due to regularization; $\widehat{\mathbf{k}_s}$ = regularized sectional stiffness; $\widetilde{\mathbf{k}_s}$ = additional contribution to the sectional stiffness due to regularization; and $\mathbf{a_s}$ = sectional kinematic matrix that describes the strain distribution in the local coordinates.

Regularization of Concrete in Compression

The concept of constant fracture energy of concrete in compression is defined as in Eq. (9) based on Coleman and Spacone (2001)

$$G_f^c = \int \sigma du \tag{9}$$

where G_f^c = fracture energy of concrete, where superscript c represents compression; and σ and u = stress and inelastic displacement, respectively. The approach is adapted to a framework of stress and strain by expressing the fracture energy as follows:

$$G_f^c = h\int \sigma d\varepsilon \tag{10}$$

$$G_f^c = L_{\mathrm{IP}}\int \sigma d\varepsilon \tag{11}$$

where h = length scale representing the size of a single element. For a force-based element, h becomes the length associated with an

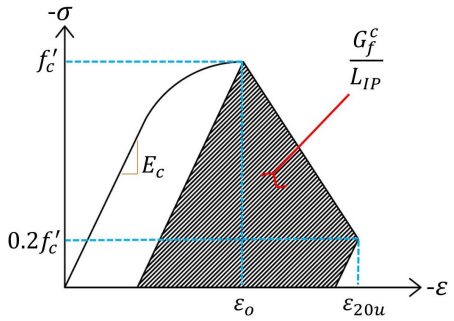

Fig. 2. Regularized compressive concrete response.

individual integration point at the presence of a softening response (L_{IP}). Fig. 2 shows the stress-stain relation and fracture energy in compression. The regularization is applied to the Kent and Park (1971) concrete model, and fracture energy of concrete is defined from the peak compressive stress until the end of the softening branch shown in the shaded area in Fig. 2, where f_c' denotes the compressive strength of unconfined concrete, E_C is the elastic modulus, ε_O is the strain corresponding to peak stress, and ε_{20u} is the strain corresponding to 20% f_c'.

In order to implement the regularization process, the compressive fracture energy of concrete needs to be estimated. The authors refer to the few studies found in the literature to obtain this estimate. From Coleman and Spacone (2001), the fracture energy of plain concrete obtained from cylinder tests gives values of 20–30 N/mm. Due to the confining effect of steel hoops, the compressive fracture energy of well-confined concrete increases to about 180 N/mm, or six times that of unconfined concrete. Jansen and Shah (1997) recommended the use of a value of 25 N/mm for normal-weight concrete. Coleman and Spacone (2001) used this same value for unconfined concrete and a value of $6G_f^c$ for a confined concrete material. Due to the lack of literature regarding the fracture energy for partially confined concrete, the current study assumes that concrete is either unconfined for the concrete cover with a fracture energy value of 25 N/mm, or well-confined for the concrete core with a fracture energy value of 150 N/mm. Finally, modification of the concrete material is done by adjusting the strain ε_{20u} to ensure constant energy release, resulting in Eq. (12)

$$\varepsilon_{20u} = \frac{G_f^c}{0.6 f_c' L_{\text{IP}}} - \frac{0.8 f_c'}{E_C} + \varepsilon_O \tag{12}$$

The regularization of concrete in tension is neglected in this study because the concrete tensile response has minimal influence on the softening behavior of the concrete section.

Regularization of Lap Splice in Tension

To approach regularization of the material behavior in the lap-splice region, it is important to look at the constitutive material and failure mechanism of lap splices. This study combines findings from several previous studies to obtain the constitutive material model of the splice. The mechanism transferring the tensile stress in the splice relies on the concrete tensile stress capacity. The concrete acts as an intermediate material that transfers forces between two adjacent bars (Priestley et al. 1996). Splitting cracks along the bar in concrete can be formed due to the stress-transferring mechanism, which causes radially outward pressure on the concrete. The cracking of the concrete in tension causes initiation of softening due to degrading behavior of the lap-spliced reinforcement (Wight and MacGregor 2009). In addition to inadequate lap-splice length, widely spaced transverse steel bars in the lap-splice region further reduce ductility of the column response once cover concrete has spalled.

To assess the stress-strain relation for lap splices, this paper uses the relation proposed by Priestley et al. (1996) to obtain the value of maximum force and stress developed in the lap-splice region, as shown in Eqs. (13) and (14), respectively

$$T_b = A_b f_s = F_t p L_s \tag{13}$$

$$f_s = \frac{F_t p L_s}{A_b} \tag{14}$$

where T_b and f_s = force and stress developed in the lap-spliced bar, respectively; A_b = cross-sectional area of longitudinal bar; F_t = tensile strength of concrete; L_s = length of lap splice; and p = perimeter of the cylindrical block, which is determined through Eq. (15) with an upper limit for widely spaced spliced bars

$$p = \frac{s}{2} + 2(d_b + c) \le 2\sqrt{2(c + d_b)} \tag{15}$$

where s = average distance between spliced bars; d_b = diameter of longitudinal steel bar; and c = thickness of concrete cover. Residual stress f_r is computed after the lap splice reaches its peak stress f_s as by Tariverdilo et al. (2009) and shown in Eq. (16)

$$f_r = \frac{n_1 n_t \mu A_h f_s}{n A_b} \tag{16}$$

where n_1 = number of transverse reinforcement legs perpendicular to the crack plane; n_t = number of transverse reinforcements in lap-splice length; μ = frictional factor, which is taken as 1.4; A_h = cross-sectional area of transverse reinforcement; and n = number of spliced longitudinal bars developed by friction stress in the crack plane. Slip corresponding to maximum stress is assumed to be 1 mm and slip corresponding to reaching frictional stress is 10 mm as in Tariverdilo et al. (2009). As a result, residual strain ε_r is set to be 0.022 and peak strain ε_s can be obtained from Eq. (17)

$$\varepsilon_s = \frac{f_s}{E_s} + \frac{\Delta_{\text{BarSlip}}}{l_{ss}} \tag{17}$$

where E_s = elastic modulus of steel bar; Δ_{BarSlip} at peak stress is taken as 1 mm; and l_{ss} = length in which displacement due to slip occurs and is taken as section depth. The compression side of the reinforcement is assumed to follow perfectly plastic behavior. Based on Eqs. (13)–(17), the stress-strain curve is illustrated in Fig. 3.

To obtain the postpeak energy value, this study considers six experimental specimens from Melek and Wallace (2004) and Aboutaha et al. (1996). These column specimens consist of either square or rectangular cross-sections and lap-splice lengths of $20 \times d_b$ or $24 \times d_b$. Column geometries and material properties are listed in Tables 1 and 2, respectively.

Fig. 4 shows the formulation for regularizing the tensile lap-splice response. From Fig. 4, the constant postpeak energy of the lap-splice region in tension is computed based on the total shaded area as shown in Eq. (18)

$$G_{\text{LS}}^T = L_{\text{IP}} \int_{\varepsilon_s}^{\varepsilon_{\text{ult}}} \sigma d\varepsilon \tag{18}$$

where superscript T = tension; and subscript LS = lap splice. G_{LS}^T consists of two portions as indicated in Fig. 4. The two portions are calculated according to Eqs. (19) and (20)

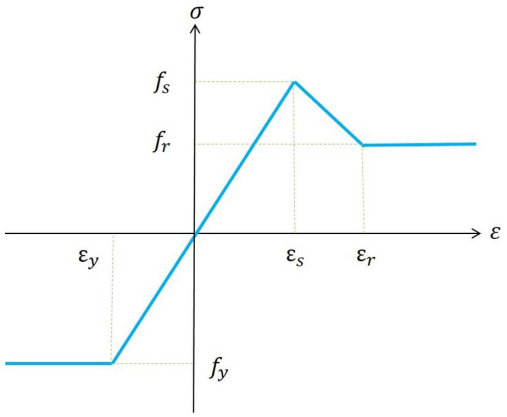

Fig. 3. Constitutive material model of lap-spliced bar.

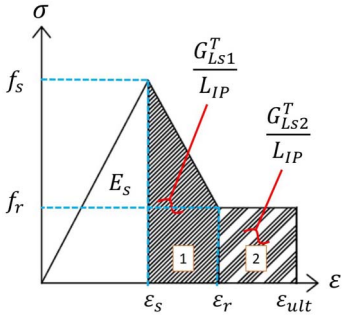

Fig. 4. Regularized tensile lap-splice response.

Table 1. Experimental column specimen geometries and axial load ratios

Specimen	Column dimensions			Shear span ratio	Axial load ratio
	Width (mm)	Depth (mm)	Height (mm)		
FC4	914	457	2,743	3.00	0
FC14	686	457	2,743	4.00	0
FC15	457	457	2,743	6.00	0
S10MI	457	457	1,829	4.00	0.10
S20MI	457	457	1,829	4.00	0.20
S30MI	457	457	1,829	4.00	0.30

$$G^T_{\mathrm{LS1}} = \frac{1}{2}(\varepsilon_r - \varepsilon_s)(f_s + f_r)L_{\mathrm{IP}} \tag{19}$$

$$G^T_{\mathrm{LS2}} = (\varepsilon_{\mathrm{ult}} - \varepsilon_r)f_r L_{\mathrm{IP}} \tag{20}$$

where $\varepsilon_{\mathrm{ult}}$ = ultimate strain of the lap-splice section with the value taken to be 0.08.

The other parameters needed to calculate the postpeak energy are computed based on the material stress-strain relations of Tariverdilo et al. (2009). The resulting parameter values are shown in Table 3. Tariverdilo et al. (2009) took two Gauss-Labatto integration points at the lap section to result in sufficient accuracy compared with experimental results. Therefore, the integration length L_{IP} is set equal to half of the lap-splice length. The resulting postpeak energies G^T_{LS1} and G^T_{LS2} calculated for each specimen based on the proposed Eqs. (19) and (20) are given in Table 3.

The mean values for G^T_{LS1} and G^T_{LS2} are calculated over the six lap-splice column specimens as 1,258 and 1,886 N/mm, respectively. These values are used to obtain the regularized residual strain ($\widetilde{\varepsilon_r}$) and regularized ultimate strain ($\widetilde{\varepsilon_{\mathrm{ult}}}$) as shown in Eqs. (21) and (22)

$$\widetilde{\varepsilon_r} = \frac{\overline{G^T_{\mathrm{LS1}}}}{L_{\mathrm{IP}}}\frac{2}{f_s + f_r} + \varepsilon_s \tag{21}$$

$$\widetilde{\varepsilon_{\mathrm{ult}}} = \frac{\overline{G^T_{\mathrm{LS2}}}}{L_{\mathrm{IP}} f_r} + \widetilde{\varepsilon_r} \tag{22}$$

where $\overline{G^T_{\mathrm{LS1}}}$ and $\overline{G^T_{\mathrm{LS2}}}$ = average values of postpeak energy for short lap splices.

For Eqs. (21) and (22), the regularized residual strain is determined first based on the average value of G^T_{LS1}. The regularized ultimate strain is then obtained by adding the strain contribution based on the average value of G^T_{LS2}. Fig. 5 shows regularized stress-strain curves of a lap splice in tension considering varying numbers of integration points with constant postpeak energy. Here, $\widetilde{\varepsilon_{r\_2\mathrm{IP}}}$, $\widetilde{\varepsilon_{r\_3\mathrm{IP}}}$, and $\widetilde{\varepsilon_{r\_4\mathrm{IP}}}$ represent regularized residual strains with two, three, and four integration points along the element, respectively. Likewise, $\widetilde{\varepsilon_{\mathrm{ult}\_2\mathrm{IP}}}$, $\widetilde{\varepsilon_{\mathrm{ult}\_3\mathrm{IP}}}$, and $\widetilde{\varepsilon_{\mathrm{ult}\_4\mathrm{IP}}}$ represent regularized ultimate strains with two, three, and four integration points along the element, respectively.

Modeling Details

To evaluate the proposed regularization approach to model the lap-splice material response, the authors build a numerical column model simulating lap-splice failure. The finite-element model of the reinforced concrete column with lap splice at the base consists of two force-based beam-column elements with fiber discretization connected in series. The deformation of the lapped region due to bar slip and column flexural behavior is captured by the bottom element with a length set equal to the actual length of splice; the flexural behavior of the remaining portion of the column is captured by the top element. The model is implemented in the finite-element platform OPENSEES version 3.2.0 (McKenna 1997).

Table 2. Experimental column specimen material properties

Specimen	Longitudinal reinforcement			Transverse reinforcement		Concrete compressive strength (MPa)
	No.	Lap-splice length (d_b)	Yield strength (MPa)	Spacing (mm)	Yield strength (MPa)	
FC4	16#8	24	434	#3@406	400	19.7
FC14	12#8	24	434	#3@406	400	28.8
FC15	8#8	24	434	#3@406	400	28.8
S10MI	8#8	20	510	#3@305	476	36.3
S20MI	8#8	20	510	#3@305	476	36.3
S30MI	8#8	20	510	#3@305	476	36.3

Table 3. Material parameters and resulting postpeak energy

Specimen	f_s/f_y	f_r/f_y	ε_s	ε_r	G_{LS1}^T (N/mm)	G_{LS2}^T (N/mm)
FC4	0.79	0.25	0.0039	0.022	1,246	1,920
FC14	0.95	0.26	0.0043	0.022	1,418	1,997
FC15	0.95	0.20	0.0042	0.022	1,348	1,536
S10MI	0.78	0.26	0.0042	0.022	1,195	1,954
S20MI	0.78	0.26	0.0042	0.022	1,195	1,954
S30MI	0.78	0.26	0.0042	0.022	1,195	1,954
Mean postpeak energy (N/mm)					1,258	1,886

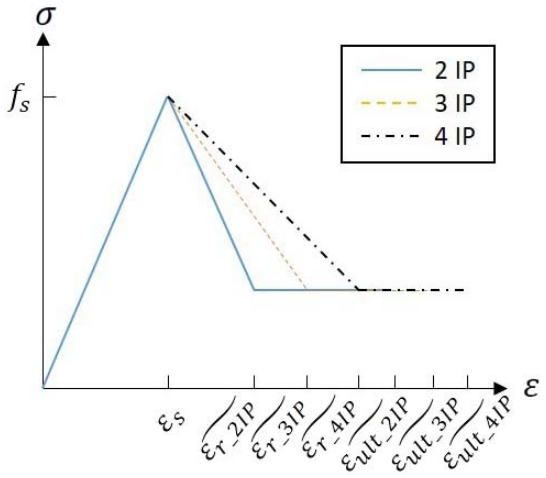

Fig. 5. Regularized constitutive relation of lap-splice response with varying numbers of integration points.

The uniaxial stress-strain relation of the longitudinal reinforcement in the lap-splice region adopts the stress-strain curve shown in Fig. 3. It is implemented by using material model Hysteretic in OPENSEES, which is capable of modeling the trilinear stress-strain relation depicted in Fig. 3. The ultimate tensile strain of lap splices is implemented through material model MinMax in OPENSEES. The longitudinal reinforcement in the top element uses a steel element with material model Steel01 in OPENSEES, which consists of bilinear behavior with kinematic hardening. Yield strength and ultimate strength are based on the material properties of each specimen. For the concrete material, the model from Yassin (1994) is adopted, which is implemented as Concrete02 in OPENSEES. From Yassin (1994), the model from Hognestad (1951) is used for prepeak behavior. The stress-strain curve between the concrete compressive strength and crushing strength is assumed to be linear, with the crushing strength assumed to be 20% of maximum compressive strength. The initial slope for the concrete model is $2f_c'/\varepsilon_o$, where f_c' and ε_o are concrete compressive strength and concrete strain at maximum strength, respectively.

The unloading path from the compression envelope and tension envelope is bilinear and linear, respectively. The reloading path is assumed to be linear. Compressive strength is defined according to the material properties of each specimen, and the concrete modulus is computed based on ACI (2011). For the confined concrete model, the same uniaxial material model Concrete02 is adopted. However, the maximum confined concrete stress and its corresponding strain are computed based on Mander et al. (1988). Fig. 6 shows the 1D constitutive models used for the steel and concrete materials.

The proposed regularization process for the material response is implemented for the described numerical model. As shown in Fig. 7, the top element of the column model has three Gauss-Lobatto integration points; the bottom element has two integration points. Ls_{IP} indicates the integration length of the lapped region, and L_{upper} is the length of the upper element excluding the lapped region. The number of integration points in the bottom element is varied in the next section to investigate objectivity of the results with and without using the regularized concrete and lap-splice material models.

Theoretically, the proposed regularized strains should apply to each integration point. However, because the plastic hinge region is typically at the end of the element, the regularization is applied only to the extreme integration point in this paper. Implementing the regularization at the other integration points does not significantly affect the results.

Evaluation of Results with Proposed Regularization

In this section, the authors present results for five column specimens with short lap splices. Summary results in terms of estimating the displacement at 20% strength drop for the five specimens using a regularized compared with a nonregularized model and compared with experimental tests are presented to demonstrate generalizability and utility of the proposed approach. Detailed results are then

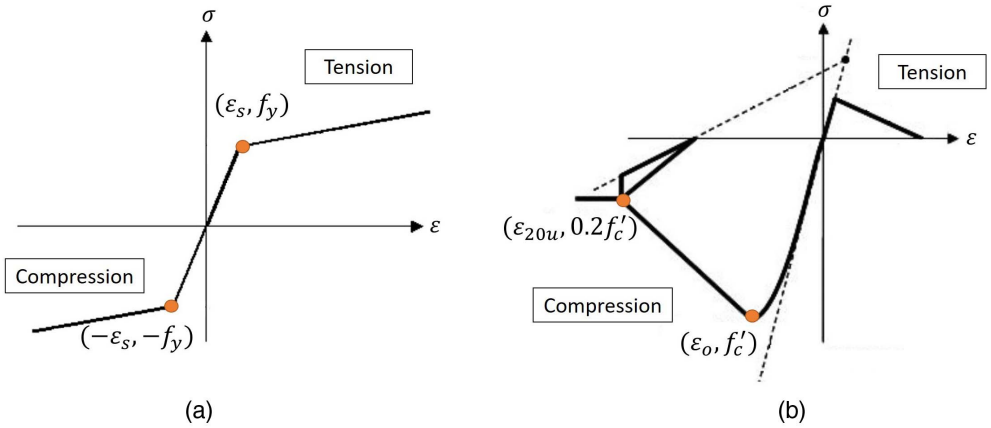

Fig. 6. One-dimensional constitutive models used for (a) steel material; and (b) concrete material.

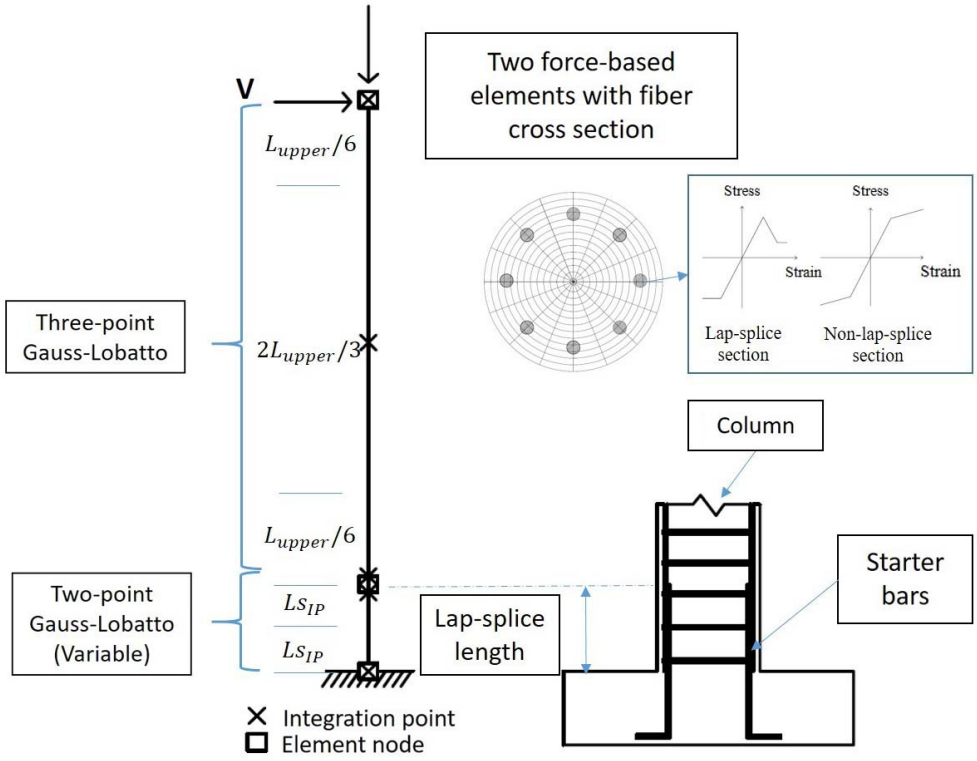

Fig. 7. Modeling details of numerical model.

Table 4. Experimental column specimen geometries and axial load ratios

Specimen	References	Column dimensions			Shear span ratio	Axial load ratio
		Width (mm)	Depth (mm)	Height (mm)		
1	Sun et al. (1993)	1,830	1,220	9,140	4.99	0.15
2	Chail et al. (1991)	610[a]	—	3,660	6.00	0.18
3	T1 of Jaradat et al. (1998)	250[a]	—	1,780	3.56	0.05
4	T2 of Jaradat et al. (1998)	250[a]	—	1,780	3.56	0.05
5	2S20H of Melek and Wallace (2004)	457	457	1,676	3.67	0.20

[a]Circular cross section.

described for two out of the five specimens, with the figures for the remaining specimens provided in the Appendix for concision. In the analyses, the goal is to evaluate objectivity of the proposed regularization approach across integration points and verify the accuracy of the regularized model compared with experimental tests. Results for pushover, static cyclic, and dynamic analyses are presented.

Descriptions of Test Specimens

Five test specimens are selected for evaluation of the proposed regularization approach. These specimens are chosen due to the availability of experimental test data for comparison. Tables 4 and 5 provide the geometries, axial load ratios, and material properties of each specimen. The test specimens consist of rectangular, square, and circular cross sections. Specimen 1 and Specimen 2 are from Sun et al. (1993) and Chail et al. (1991), respectively. Specimen 3 and Specimen 4 are from Jaradat et al. (1998), with Specimen 3 corresponding to Specimen T1 and Specimen 4 corresponding to T2 in the study. Specimen 5 is from Melek and Wallace (2004), corresponding to Specimen 2S20H. The specimens have a lap-splice length of 20 times the longitudinal bar diameter. Transverse reinforcement of the specimens is widely spaced with average ratio of 0.2%. The shear span ratios of greater than 3.5 for all specimens ensures sufficient shear strength at the base of the column such that lap-splice failures will result.

Summary of Results for Test Specimens

Fig. 8 provides a summary of the accuracy of the regularized model compared with the nonregularized model in terms of normalized displacement at 20% strength drop for different numbers of integration points used in the analysis. Fig. 8(a) shows the results for all five test specimens. The normalization is computed as the ratio between the numerical and experimental results to assess accuracy of the model compared with experimental tests. Fig. 8(b) provides the mean values over the five specimens. The results show that the accuracy of the nonregularized model heavily depends on the number of integration points, with poor accuracy when the number of integration points exceeds two, as may be desired for longer specimen lengths. The nonregularized models show less than 50% accuracy once three or more integration points are used

Table 5. Experimental column specimen material properties

Specimen	Longitudinal reinforcement			Transverse reinforcement		Concrete compressive strength (MPa)
	No.	Lap-splice length (d_b)	Yield strength (MPa)	Spacing (mm)	Yield strength (MPa)	
1	32#6	20	317	#2 @ 127	276	33.0
2	26#6	20	315	#2 @ 127	350	34.0
3	8#4	20	360	9 gauge @ 98[a]	210	29.0
4	8#3	20	350	9 gauge @ 98[a]	210	29.0
5	8#8	20	510	#3 @ 305	476	36.3

[a]9-gauge steel with diameter of 3.8 mm.

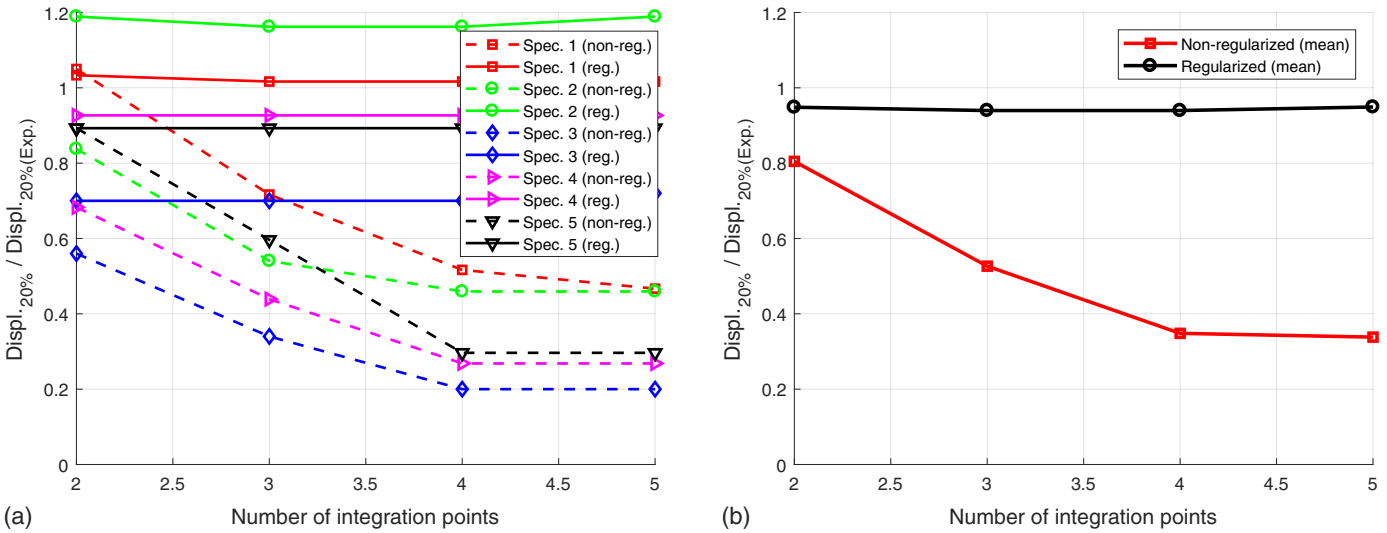

Fig. 8. Normalized displacement at 20% strength drop versus number of integration points between regularized and nonregularized models: (a) all five test specimens; and (b) mean values.

in the lapped region. This decrease in accuracy is typical when existing approaches are used. In comparison, the accuracy from using the regularized models remains constant regardless of the number of integration points. The mean accuracy of the response using the regularized model is 94% compared with the experimental tests.

The following sections provide detailed results for two specimens, Specimen 1 and Specimen 2 from Table 4. Figures for the other specimens are provided in the Appendix. Specimen 1 is from Sun et al. (1993), which is designed based on a prototype rectangular column with dimensions of 1.83, 1.22, and 9.14 m for section depth, section width, and column height, respectively. The actual test specimen uses a scale factor of 40% of the prototype, which results in a 730 × 489 mm cross section and 3.66 m column height. The column consists of 32 M22 (No. 6) longitudinal bars and 6.4 mm (No. 2) transverse reinforcement with spacing at 127 mm. The cover concrete is 19 mm, and an axial load of 1,780 kN is applied to the column at the top resulting in an axial load ratio of 15%. The concrete compressive strength is 33 MPa; the yield strength and ultimate strength of the longitudinal steel are 317 and 476 MPa, respectively. Lap splices at the base have a length of 381 mm, which is around 20 times the longitudinal bar diameter.

Specimen 2 is from Chail et al. (1991). The test specimen has a circular cross section with a diameter of 610 mm and height of 3.66 m. The longitudinal reinforcement consists of 26 No. 6 steel bars, and the transverse reinforcement consists of No. 2 bars at 127 mm spacing. The cover concrete is 20 mm, and an axial load of 2,758 kN is applied to the column at the top resulting in an axial load ratio of 17.7%. The concrete compressive strength is 34 MPa; the yield strength and ultimate strength of the longitudinal steel are 315 and 498 MPa, respectively. Lap splices at the base have a length of 381 mm, which is around 20 times the longitudinal bar diameter.

Static Pushover Analysis: Nonregularized versus Regularized Model

To assess the nonlinear behavior of the specimens, pushover analyses with a displacement control strategy are performed in OPENSEES. The parameters that are considered for comparison include the number of Gauss integration points in the lap-splice region both with and without implementing the proposed regularized lap-splice material model. Pushover results for Specimen 1 and Specimen 2 are shown in Figs. 9(a and b) and 9(c and d), respectively, with applied maximum drift ratio of 2% in both cases.

Figs. 9(a and c) show the pushover curves without implementing the proposed regularized material model. The analyses in the lap-splice region exhibit different levels of premature degrading behavior depending of the number of IPs due to strain localization beginning at 0.8% and 0.6% drift ratio for Specimen 1 and Specimen 2, respectively. The analysis results thus highly depend on the number of integration points used by the analyst. However, if regularization is applied to both the concrete and lap-splice constitutive material models, convergent and objective structural responses are observed. Table 6 provides the drift ratios at 20% drop of lateral strength between the regularized and nonregularized models for the two specimens.

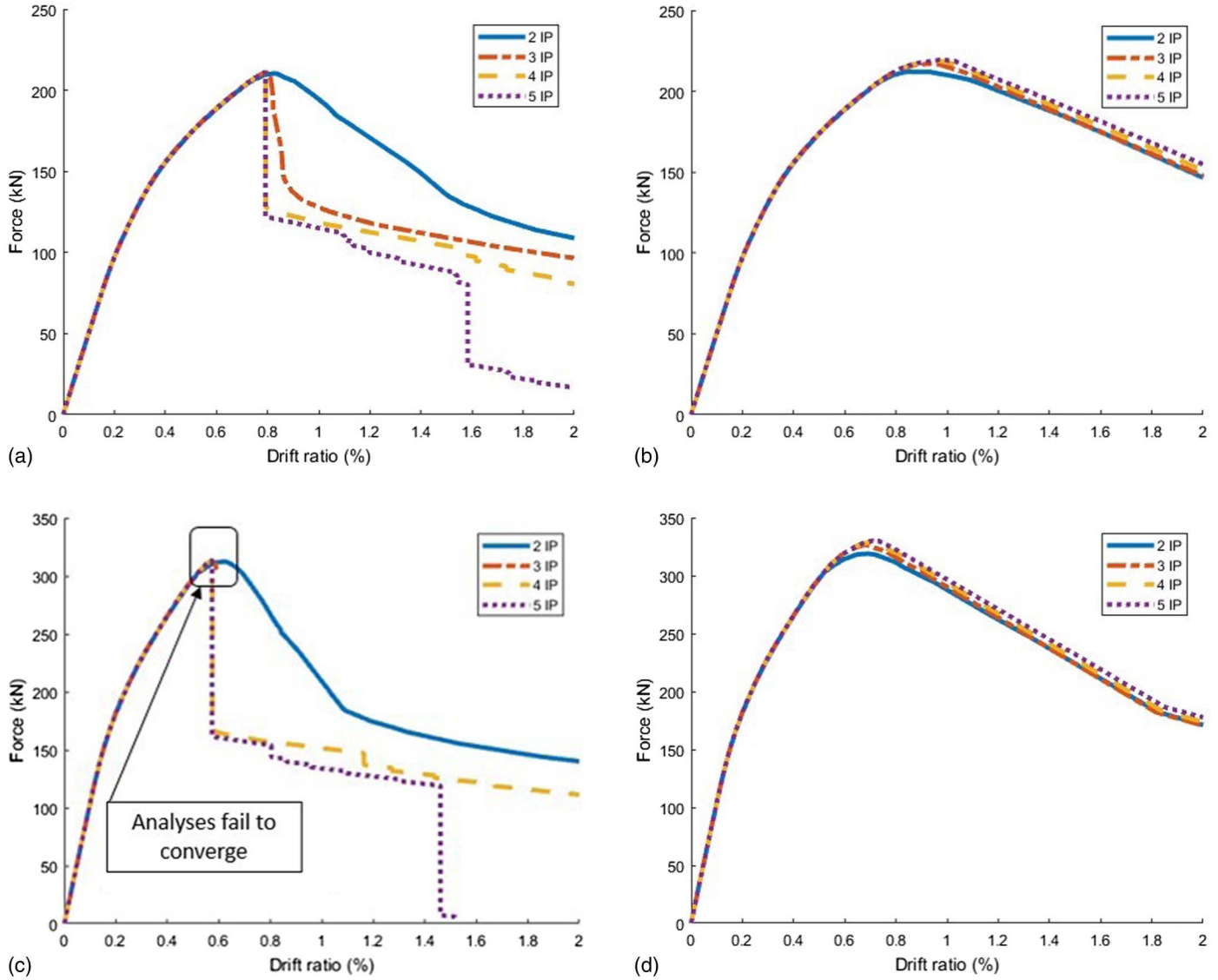

Fig. 9. Static pushover curves for varying numbers of integration points in the lap-splice region: (a and c) nonregularized responses; and (b and d) regularized responses.

Table 6 quantifies the difference between the results obtained from using the nonregularized compared with regularized models in terms of drift ratio at 20% strength drop as the number of integration points varies. The nonregularized results show large variation in drift ratio depending on the number of integration points used. In contrast, results indicate that the regularized model is able to eliminate the issue of premature degrading due to strain localization, reducing the standard deviation of drift ratio at 20% strength drop from 0.18% and 0.12% to 0.02% and 0.02% for the two specimens, respectively. The decrease in standard deviation of the response combined with the results shown in Figs. 9(b and d) indicate that the regularization alleviates the issue of convergence. The pushover curves become objective with results independent of the number of integration points used.

Table 6. Pushover values for test specimens using nonregularized versus regularized models

Number of integration points	Drift ratio at 20% strength drop (%)			
	Specimen 1		Specimen 2	
	Nonregularized model	Regularized model	Nonregularized model	Regularized model
2	1.22	1.65	0.85	1.25
3	0.85	1.60	—	1.21
4	0.80	1.59	0.59	1.20
5	0.80	1.59	0.59	1.20
Mean	0.92	1.61	0.68	1.22
Standard deviation	0.18	0.02	0.12	0.02

Note: Dash indicates analysis fails to converge.

Static Cyclic Analysis: Nonregularized versus Regularized Model

Cyclic loadings are also applied to assess performance of the regularized compared with nonregularized models. A lateral displacement cycle of prescribed magnitude is imposed at the top of the column node using the displacement control integrator in OPENSEES. The numerical models are subjected to the same displacement pattern of increasing magnitude in accordance with

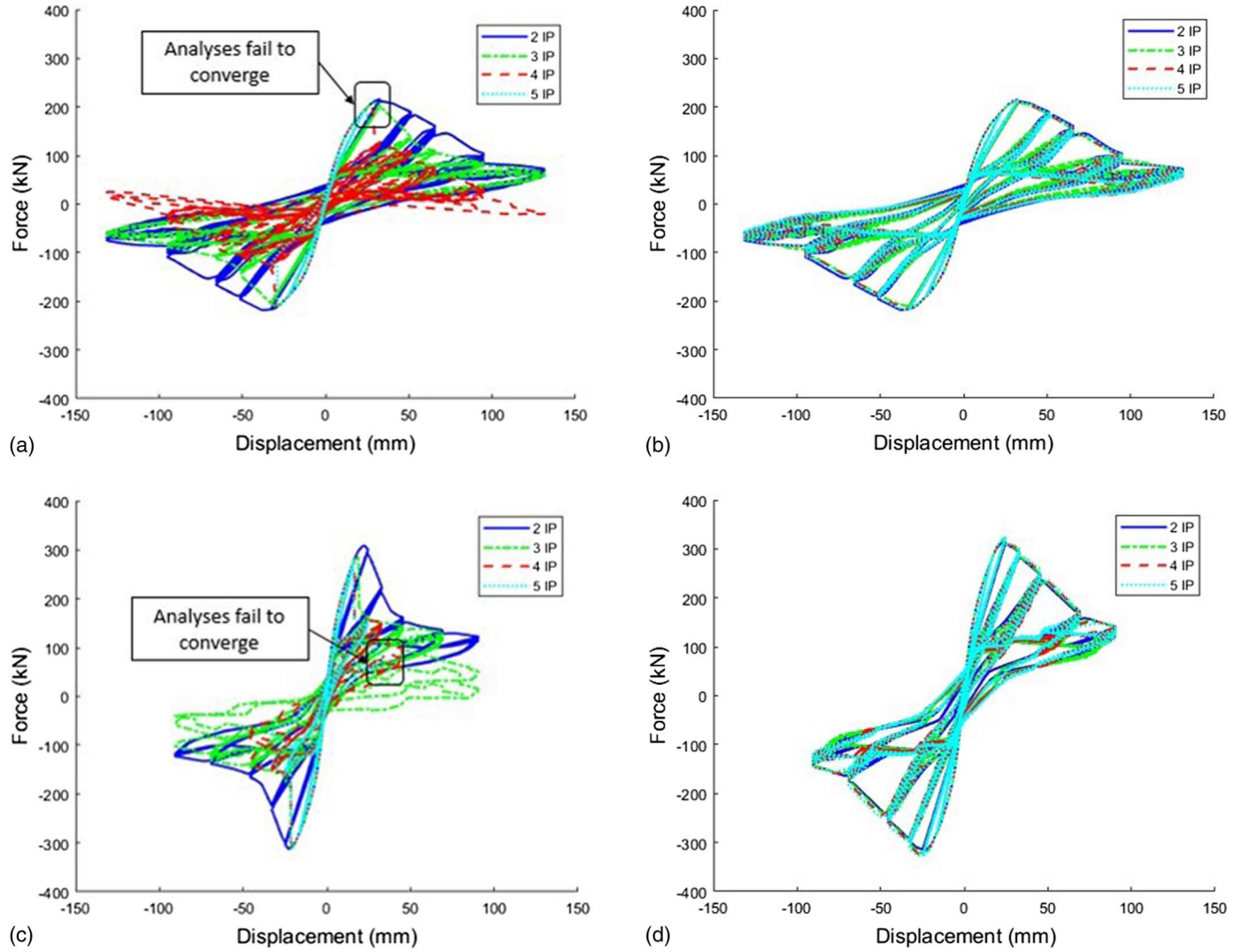

Fig. 10. Static cyclic curves of (a and c) nonregularized responses; and (b and d) regularized responses.

the experimental tests. The study uses an adaptive strategy, which tries multiple solution algorithms, including Newton-Raphson, modified Newton-Raphson, Newton with linear search, and so on, before it fails to converge. The resulting static cyclic curves are shown in Fig. 10 for both specimens with and without considering regularization. The results from Specimen 1 and Specimen 2 are shown in Figs. 10(a and b) and 10(c and d), respectively.

Figs. 10(a and c) show the static cyclic curves for the two specimens when different numbers of integration points are used without regularization. Both cases show that the results vary based on the number of integration points in the model. The analyses using more integration points degrade faster, and the issue of convergence persists due to the decrease of integration weight as the number of integration points along bottom the element increases. The difference in integration weight leads to variations in the element deformation $\mathbf{v}$ during element-state determination. Without the regularization, the results become nonobjective because they depend on the number of integration points used by the analyst.

Table 7. Static cyclic values for Specimen 1

	Nonregularized model		Regularized model	
Number of integration points	Peak strength (kN)	Displacement at 20% strength drop (mm)	Peak strength (kN)	Displacement at 20% strength drop (mm)
2	216	63	216	62
3	208	43	210	61
4	203	31	215	61
5	195	28	216	61
Mean	206	41	214	61
Standard deviation	7.63	13.75	2.49	0.43

Table 8. Static cyclic values for Specimen 2

	Nonregularized model		Regularized model	
Number of integration points	Peak strength (kN)	Displacement at 20% strength drop (mm)	Peak strength (kN)	Displacement at 20% strength drop (mm)
2	308	31	315	44
3	286	20	322	43
4	280	17	324	43
5	280	17	325	44
Mean	289	21	322	44
Standard deviation	11.52	5.76	3.91	0.50

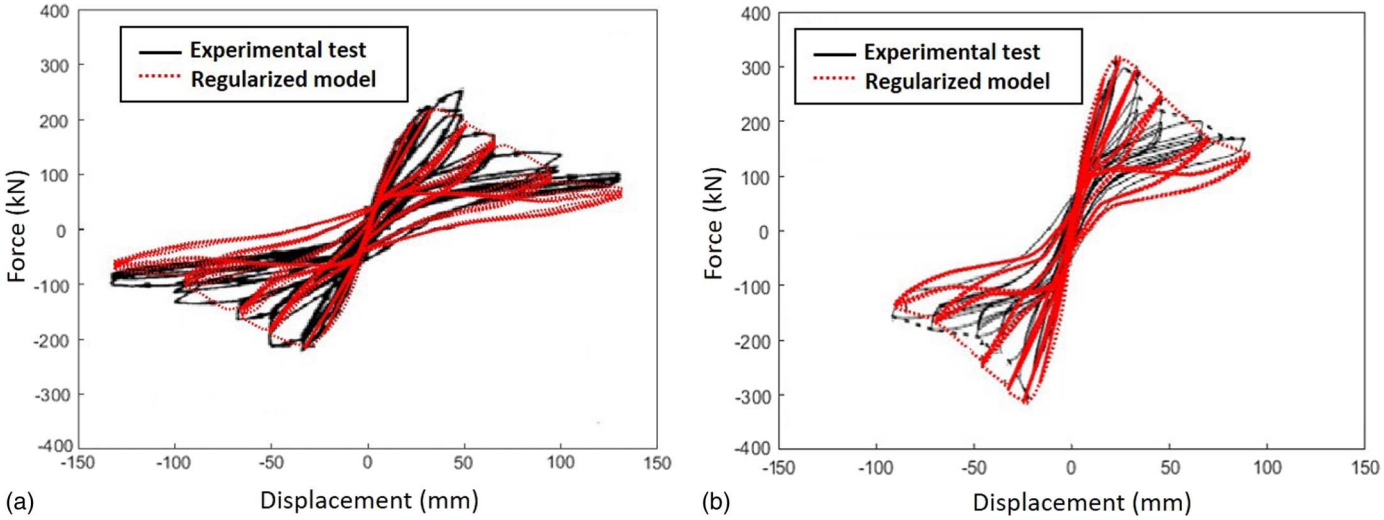

Fig. 11. Experimental test results compared with regularized numerical model results: (a) Specimen 1; and (b) Specimen 2.

Table 9. Comparison between experimental tests and regularized model results

Models and difference	Specimen 1		Specimen 2	
	Peak strength	Displacement at 20% strength drop	Peak strength	Displacement at 20% strength drop
Experimental test	218 kN	60 mm	300 kN	37 mm
Regularized model	214 kN	61 mm	322 kN	43 mm
Difference (%)	1.83	1.67	7.33	16.22

In comparison, Figs. 10(b and d) show that the static cyclic curves from using the regularized model for both specimens are free from the strain localization and convergence issues. The results are consistent across varying numbers of integration points and converge in all cases.

Tables 7 and 8 quantify the differences between the regularized and nonregularized models across different integration points for Specimen 1 and Specimen 2, respectively. Results for the peak strength and displacement at 20% strength drop are shown. For both response parameters and both specimens, the nonregularized model leads to results with greater variation as a function of the number of integration points. The variability is significantly reduced by using the regularized model. The standard deviations of displacements at 20% strength drop are reduced from 13.75 to 0.43 mm, and from 5.76 to 0.50 mm. The reduction in variation of the response further demonstrates the numerical consistency between the results from using different numbers of integration points for the regularized model.

Verification with Experimental Test Results

The static pushover and cyclic analyses show that the model with regularization results in objective global force-displacement responses. In this section, the authors verify the accuracy of the proposed regularized model against experimental test results. Figs. 11(a and b) show the comparison between the responses from

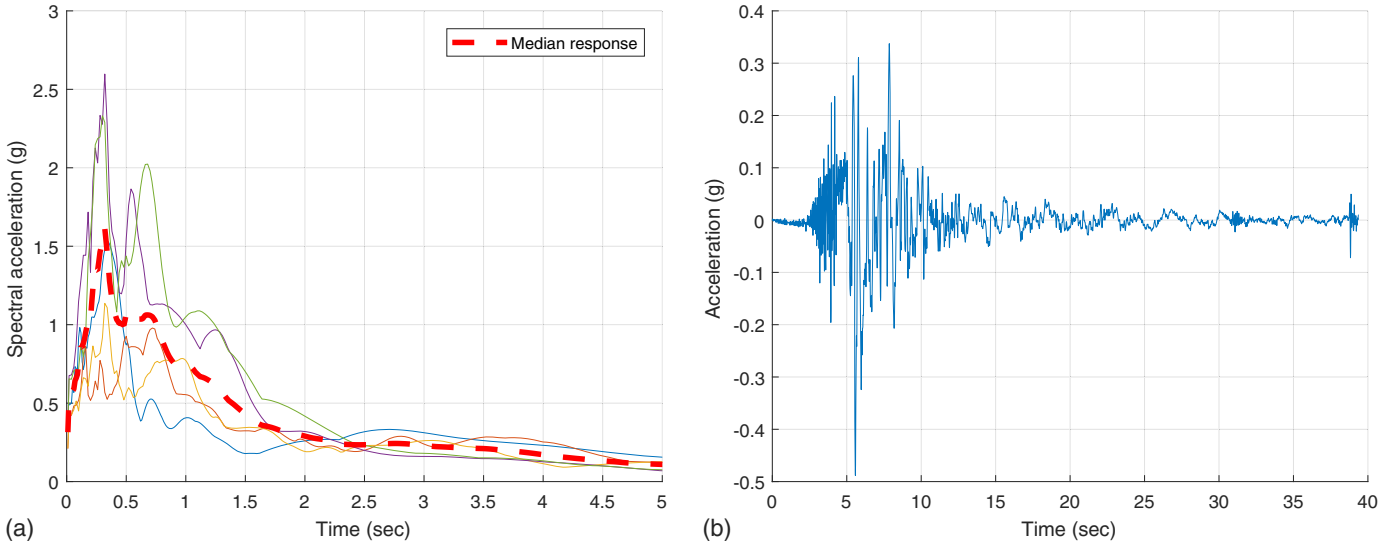

Fig. 12. (a) Response spectra of selected ground motions; and (b) time history of GM 1.

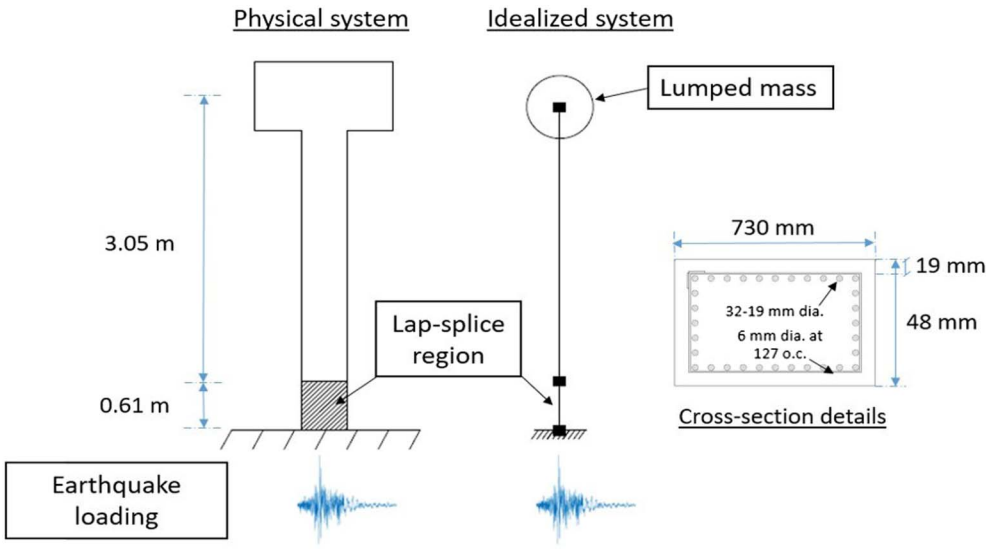

Fig. 13. Details of dynamic simulation of the test specimen.

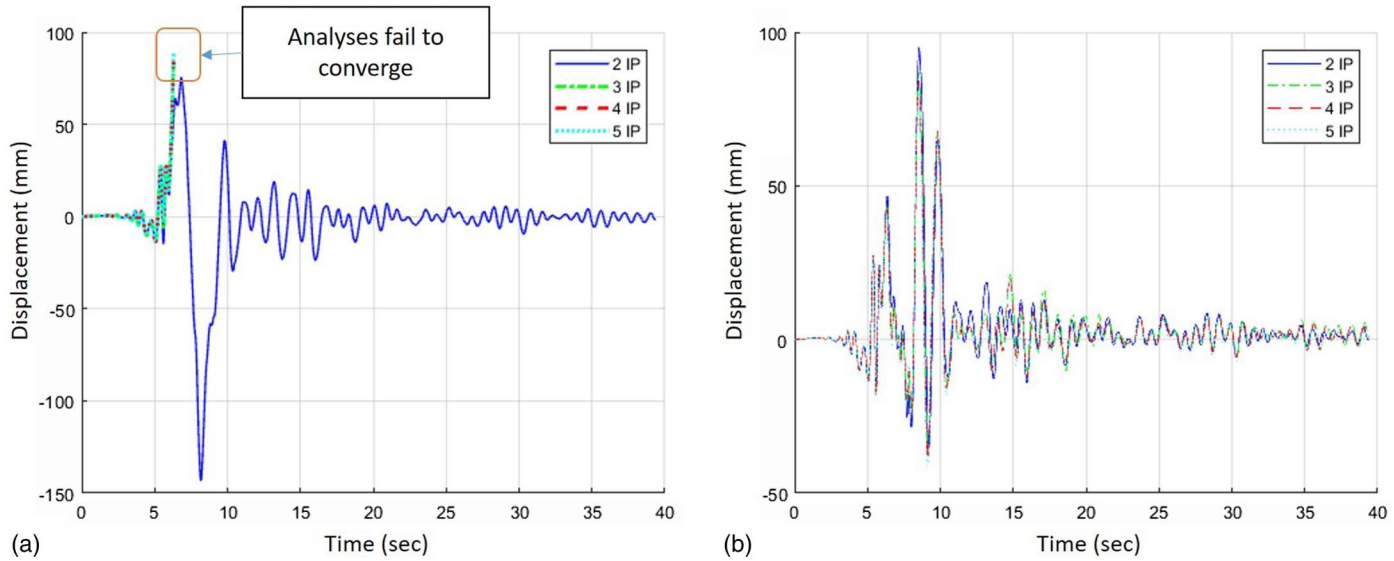

Fig. 14. Time history of column displacement: (a) nonregularized model; and (b) regularized model under GM 1.

the experimental tests and from the regularized numerical model for Specimen 1 and Specimen 2, respectively. Both specimens have bond-slip failure in the lap-splice region. From Fig. 11, the regularized models are able to model the strength, softening slope, and degrading stiffness in comparison with experimental tests.

Table 9 provides the percentage differences between the experimental tests and regularized model results in terms of peak force and displacement at 20% strength drop. The percentage differences are below 10%, except for the displacement quantity for Specimen 2 with around 16% difference. This discrepancy could be caused by measurement error of the experimental test or modeling error in terms of accuracy of the fiber uniaxial behavior and damage parameters accounting for pinching behavior (Zhang et al. 2019). In an overall sense, the regularized model is able to capture the force-displacement envelope of the lap-splice columns.

In addition to the summary of results for the five test specimens provided in Fig. 8, the figures showing the detailed results from the static cyclic analyses comparing the regularized and nonregularized models as well as the verification between the experimental tests and regularized model results for the remaining three specimens are presented in the Appendix. The results for these three

Table 10. Maximum drift ratios from nonregularized models

Nonregularized model	2 IP (%)	3 IP (%)	4 IP (%)	5 IP (%)	Mean (%)
GM1	3.97	—	—	—	3.97
GM2	4.24	—	—	—	4.24
GM3	—	—	—	—	—
GM4	6.50	—	—	—	6.50
GM5	8.93	—	—	—	8.93

Note: Dash indicates analysis fails to converge.

Table 11. Maximum drift ratios from regularized models

Regularized model	2 IP (%)	3 IP (%)	4 IP (%)	5 IP (%)	Mean (%)	Standard deviation (%)
GM1	2.60	2.37	2.30	2.24	2.38	0.16
GM2	4.74	—	4.28	3.87	4.30	0.44
GM3	—	4.95	4.59	4.91	4.82	0.20
GM4	6.61	6.64	6.70	—	6.65	0.05
GM5	7.86	7.07	6.97	6.85	7.19	0.46

specimens are similar to those presented for Specimen 1 and 2 and serve to further demonstrate the accuracy and objectivity of the results obtained from implementing the proposed methodology of regularization.

Dynamic Analysis: Nonregularized versus Regularized Model

This section evaluates the structural responses from the regularized compared with nonregularized models under dynamic loading. It investigates the convergence and objectivity of the displacement response with varying numbers of integration points in the lap-splice section. The first five ground motions from the SAC (a joint venture of the Structural Engineers Association of California, Applied Technology Council, and Consortium of Universities for Research in Earthquake Engineering) ground motion suite (Somerville et al. 1997) have been selected for this study. The response spectra of these ground motions are shown in Fig. 12(a); as an example, the time history of the first ground motion (GM 1) is shown in Fig. 12(b). Fig. 13 shows the details of the physical system and the idealized system of the structural column.

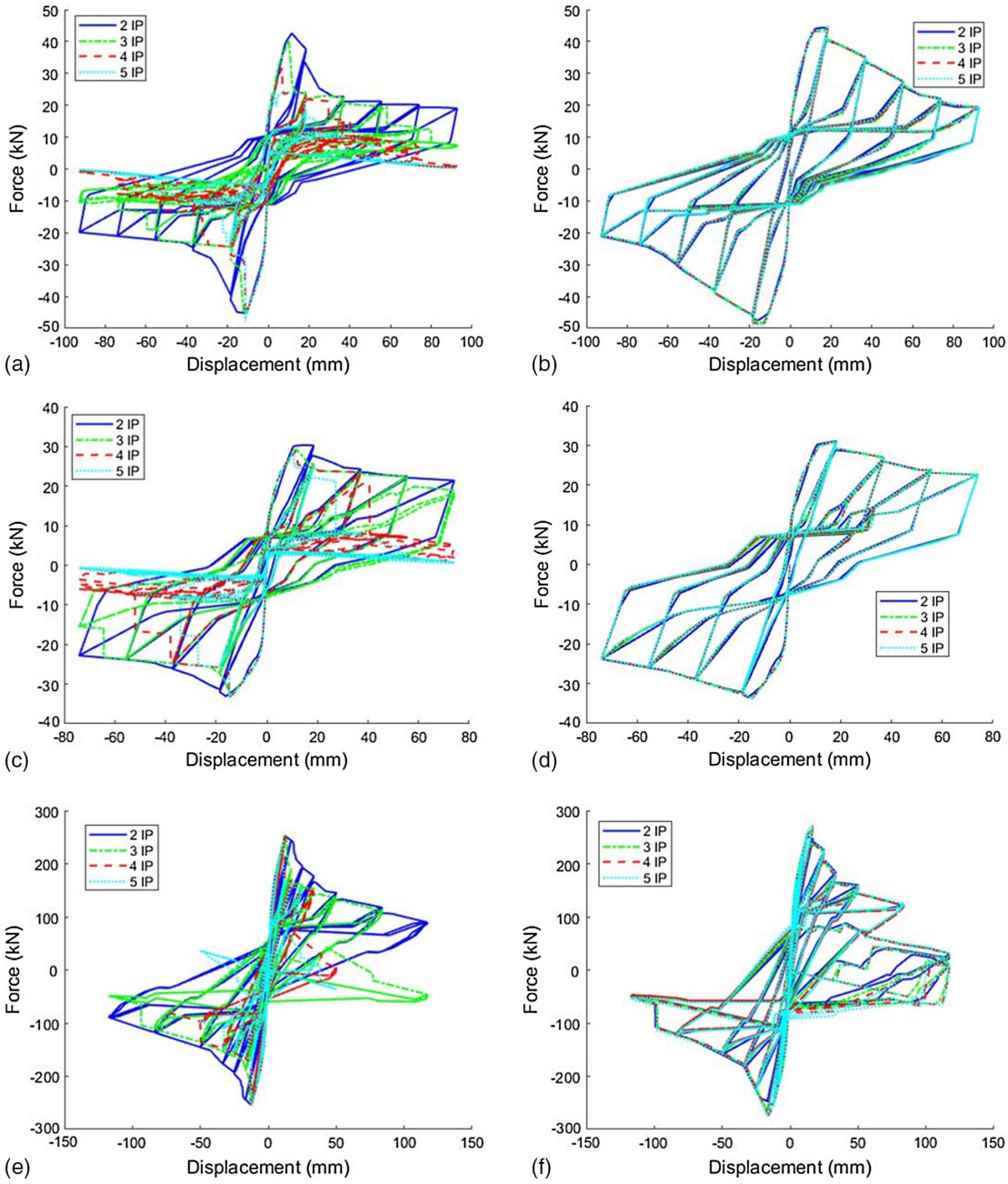

Fig. 15. (a, c, and e) Nonregularized responses; and (b, d, and f) regularized responses of Specimens 3, 4, and 5, respectively.

The structural parameters are based on those of Specimen 1. Ground excitations are applied at the base of the column.

The time history of the column tip displacement under GM 1 for the nonregularized and regularized models are shown in Figs. 14(a and b), respectively.

From Fig. 14, except for the case with two integration points in the lap-splice region, the model without considering regularization fails to converge when more than two integration points are used, and analyses halt at around 6 s due convergence issues. In comparison, the numerical model with the proposed regularization implemented has improved performance with regards to convergence, and the displacement response histories are similar regardless of the number of integration points used.

Tables 10 and 11 provide the maximum drift ratios of the nonregularized and regularized models with varying numbers of integration points in the lap-splice region under each of the five ground motions. In Table 10, it is clear that the model without considering regularization exhibits poor convergence performance when the number of integration points exceeds two in the lap-splice region. In comparison, Table 11 indicates the issue of convergence is alleviated through use of the regularized models. Although there are still cases when the analysis does not converge, most cases run successfully. Moreover, the resulting maximum drift ratios calculated from the analyses are consistent as the number of integration points changes. The average coefficient of variation of maximum drift ratio under varying numbers of integration points for these five ground motions is 5.58%.

Conclusions and Summary

This paper has proposed a methodology to regularize force-based beam-column elements for reinforced concrete columns with short lap splices at the column base. The regularization process uses a constant energy criterion to impose an extra constraint in the material uniaxial behavior, stabilizing element end deformation and element stiffness and tying material response directly to element response. Regularizing the material behavior based on a constant energy release criterion provides additional sectional stiffness that reduces both sectional deformation and section flexibility. The proposed postpeak energy of the lap-splice region is determined according to six experimental tests resulting in average values of 1,258 and 1,886 N/mm for $\overline{G^T_{\mathrm{LS1}}}$ and $\overline{G^T_{\mathrm{LS2}}}$, respectively. The regularized residual strain is then computed based on $\overline{G^T_{\mathrm{LS1}}}$, and the regularized ultimate strain determined based on the value of regularized residual strain and $\overline{G^T_{\mathrm{LS2}}}$.

The authors applied the proposed regularized constitutive material model in numerical reinforced concrete column models to evaluate performance compared with nonregularized models. Results using the nonregularized model heavily depend on the number of integration points used by the analyst. In contrast, the regularized model is able to obtain objective force-displacement results across varying numbers of integration points used, with an order of magnitude decrease in standard deviation of the response compared with the nonregularized model. In estimating the displacements at 20% strength drop, the nonregularized models show decreased accuracy compared with experimental results as the number of integration points changes, with less than 50% accuracy once three or more integration points are used in the lapped region. This decrease in accuracy is characteristic when existing nonregularized models are used. In comparison, use of the proposed regularized model results in constant response estimates regardless of the number of integration points used with a mean accuracy of

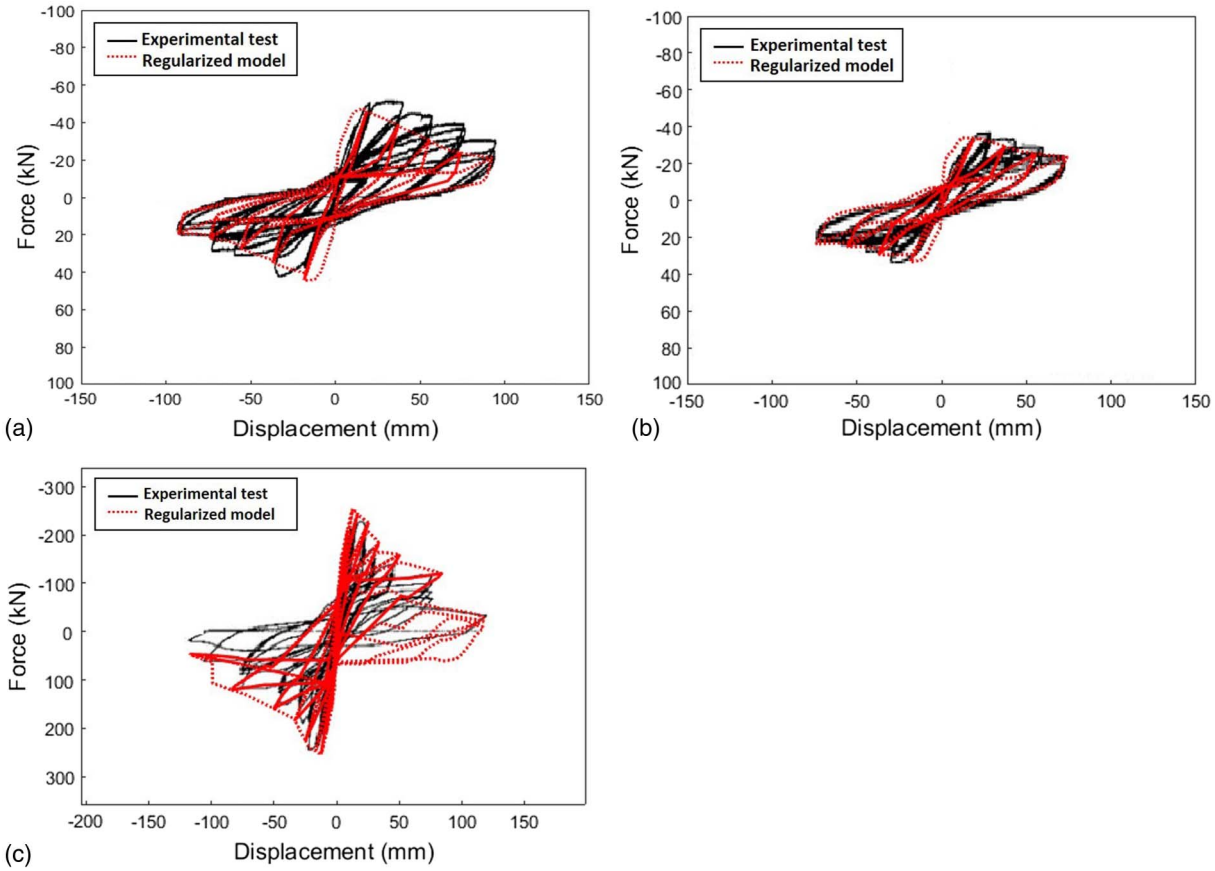

Fig. 16. Experimental test results compared with regularized numerical model results: (a) Specimen 3; (b) Specimen 4; and (c) Specimen 5.

J. Eng. Mech., 2020, 146(7): 04020073

94% for the five test specimens. The regularized model provides more accurate results against experimental data and more stable and reliable results for both static and dynamic analyses in comparison with a nonregularized model. As specimen lengths change, such as from lab-scale test specimens to the analysis of full-scale columns, the proposed regularization approach alleviates convergence issues and produces consistent results across integration points and length scales in numerical modeling and analysis.

Appendix. Additional Analysis Results

Fig. 15 shows the static cyclic analysis results for Specimens 3, 4, and 5 as described in Table 4. Comparison between the experimental tests and regularized model results for the three specimens is provided in Fig. 16.

Data Availability Statement

All MATLAB codes and OPENSEES numerical models used during the study are available from the corresponding author by request.

Acknowledgments

This project was partially funded by the INSPIRE University Transportation Center (UTC). Financial support for INSPIRE UTC projects is provided by the US Department of Transportation, Office of the Assistant Secretary for Research and Technology (USDOT/OST-R) under Grant No. 69A3551747126 through INSPIRE University Transportation Center (http://inspire-utc.mst.edu) at Missouri University of Science and Technology. The views, opinions, findings, and conclusions reflected in this publication are solely those of the authors and do not represent the official policy or position of the USDOT/OST-R, or any State or other entity.

References

Aboutaha, R. S., M. D. Engelhardt, J. O. Jirsa, and M. E. Kreger. 1996. "Retrofit of concrete columns with inadequate lap splices by the use of rectangular steel jackets." *Earthquake Spectra* 12 (4): 693–714. https://doi.org/10.1193/1.1585906.

ACI (American Concrete Institute). 2011. *Building code requirements for structural concrete and commentary.* ACI 318-14. Farmington Hills, MI: ACI.

Addessi, D., and V. Ciampi. 2007. "A regularized force-based beam element with a damage–plastic section constitutive law." *Int. J. Numer. Methods Eng.* 70 (5): 610–629. https://doi.org/10.1002/nme.1911.

Bazant, Z. P., and J. Planas. 1997. Vol. 16 of *Fracture and size effect in concrete and other quasibrittle materials*. London: CRC Press.

Bažant, Z. P., and B. H. Oh. 1983. "Crack band theory for fracture of concrete." *Matériaux et Construction* 16 (3): 155–177. https://doi.org/10.1007/BF02486267.

Chail, Y. H., M. N. Priestley, and F. Seible. 1991. "Seismic retrofit of circular bridge columns for enhanced flexural performance." *Struct. J.* 88 (5): 572–584.

Cho, J. Y., and J. A. Pincheira. 2006. "Inelastic analysis of reinforced concrete columns with short lap splices subjected to reversed cyclic loads." *ACI Mater. J.* 103 (2): 280.

Coleman, J., and E. Spacone. 2001. "Localization issues in force-based frame elements." *J. Struct. Eng.* 127 (11): 1257–1265. https://doi.org/10.1061/(ASCE)0733-9445(2001)127:11(1257).

Filippou, F. C., and G. L. Fenves. 2004. "Methods of analysis for earthquake-resistant structures." In Vol. 6 of *Earthquake engineering: From engineering seismology to performance-based engineering*, 332–410. Boca Raton, FL: CRC Press.

Hognestad, E. 1951. *Study of combined bending and axial load in reinforced concrete members.* Champaign, IL: College of Engineering, Engineering Experiment Station, Univ. of Illinois at Urbana-Champaign.

Jansen, D. C., and S. P. Shah. 1997. "Effect of length on compressive strain softening of concrete." *J. Eng. Mech.* 123 (1): 25–35. https://doi.org/10.1061/(ASCE)0733-9399(1997)123:1(25).

Jaradat, O. A., D. I. McLean, and M. L. Marsh. 1998. "Performance of existing bridge columns under cyclic loading. Part I: Experimental results and observed behavior." *Struct. J.* 95 (6): 695–704.

Kent, D. C., and R. Park. 1971. "Flexural members with confined concrete." *J. Struct. Div.* 97 (7): 1969–1990.

Lee, Y. H., and K. William. 1997. "Mechanical properties of concrete in uniaxial compression." *Mater. J.* 94 (6): 457–471.

Mander, J. B., M. J. Priestley, and R. Park. 1988. "Theoretical stress-strain model for confined concrete." *J. Struct. Eng.* 114 (8): 1804–1826. https://doi.org/10.1061/(ASCE)0733-9445(1988)114:8(1804).

McKenna, F. T. 1997. "Object-oriented finite element programming: Frameworks for analysis, algorithms and parallel computing." Ph.D. dissertation, Dept. of Civil and Environmental Engineering, Univ. of California at Berkeley.

Melek, M., and J. W. Wallace. 2004. "Cyclic behavior of columns with short lap splices." *Struct. J.* 101 (6): 802–811.

Priestley, M. N., F. Seible, G. M. Calvi, and G. M. Calvi. 1996. *Seismic design and retrofit of bridges*. New York: Wiley.

Reyes, O., and J. A. Pincheira. 1999. "R/C columns with lap splices subjected to earthquake." In *Proc., ASCE Structures Congress*, 369–372. Reston, VA: ASCE.

Scott, M. H., and O. M. Hamutçuoğlu. 2008. "Numerically consistent regularization of force-based frame elements." *Int. J. Numer. Methods Eng.* 76 (10): 1612–1631. https://doi.org/10.1002/nme.2386.

Somerville, P., N. Smith, S. Punyamurthula, and J. Sun. 1997. "Development of ground motion time histories for phase 2 of the FEMA/SAC steel project." SAC Background Document Rep. No. SAC/BD-9/04. Sacramento, CA: SAC Joint Venture.

Spacone, E., F. C. Filippou, and F. F. Taucer. 1996a. "Fibre beam–column model for non-linear analysis of R/C frames: Part I. Formulation." *Earthquake Eng. Struct. Dyn.* 25 (7): 711–725. https://doi.org/10.1002/(SICI)1096-9845(199607)25:7<711::AID-EQE576>3.0.CO;2-9.

Spacone, E., F. C. Filippou, and F. F. Taucer. 1996b. "Fibre beam–column model for non-linear analysis of R/C frames: Part II. Applications." *Earthquake Eng. Struct. Dyn.* 25 (7): 727–742. https://doi.org/10.1002/(SICI)1096-9845(199607)25:7<727::AID-EQE577>3.0.CO;2-O.

Sun, Z., M. J. N. Priestley, and F. Seible. 1993. *Diagnostics and retrofit of rectangular bridge columns for seismic loads*. San Diego: Dept. of Applied Mechanics and Engineering Sciences, Univ. of California.

Tariverdilo, S., A. Farjadi, and M. Barkhordary. 2009. "Fragility curves for reinforced concrete frames with lap-spliced columns." *Int. J. Eng. Trans. A: Basics* 22 (3): 213.

Wight, J. K., and J. G. MacGregor. 2009. *Reinforced concrete: Mechanics and designs.* 5th ed. Upper Saddle River, NJ: Prentice Hall.

Yassin, M. H. M. 1994. "Nonlinear analysis of prestressed concrete structures under monotonic and cyclic loads." Ph.D. dissertation, Dept. of Civil and Environmental Engineering, Univ. of California at Berkeley.

Zhang, Y., R. DesRoches, and I. Tien. 2019. "Impact of corrosion on risk assessment of shear-critical and short lap-spliced bridges." *Eng. Struct.* 189 (Jun): 260–271. https://doi.org/10.1016/j.engstruct.2019.03.050.